# RF Gun cavities cooling regime study.

K. Floettmann[1], V. Paramonov[2], A. Skasyrskaya[2], F. Stephan[3]

[1] - Deutsches Elektronen-Synchrotron, DESY, 22609, Hamburg, Germany
[2] - Institute for Nuclear Research of the RAS, 117312, Moscow, Russia
[3] - Deutsches Elektronen-Synchrotron, DESY, 15738, Zeuthen, Germany

## 1 Introduction

At DESY normal conducting RF Gun cavities operate with electric fields at the cathode of $E_c = 40MV/m$ or $E_c = 60MV/m$ and a pulse input RF power of $P_i \sim 3.2MW$ and $P_i \sim 6.8MW$, respectively. In combination with a long RF pulse of $\tau \sim 1ms$ and $10Hz$ repetition rate it results in average dissipated RF power of $P_a = 0.01P_i$, equal to $P_a \sim 32kW$ and $P_a \sim 68kW$.
Taking into account the cavity dimensions, the average RF power of $P_a \sim 68kW$ corresponds to a heat load of $\sim 300\frac{kW}{m}$. To remove such a high heat value from the cavity body, an advanced cooling circuit is required. The cooling circuit capability depends on the cooling channel design and the water flow parameters and finally defines the maximal possible dissipated RF power, which can be removed from the cavity and, hence, limiting the cavity duty factor.
In this report we describe a cooling circuit study for DESY RF Gun cavities N2, N3 with the aim to optimize the water flow distributions for a maximal dissipated RF power. For Gun 4, with independent cooling channels, the goal of the study is to investigate the flexibility of such a design decision.

## 2 Numerical procedure.

The basement of the numerical procedure is described in [1]. We solve steady state problems. The distribution of RF fields in the cavity at an operating frequency is calculated in the usual way. The temperature distribution $T(x, y, z)$ in the cavity body is described by the equation:

$$\mathbf{div\ k\ grad}T(x, y, z) = 0, \tag{1}$$

with the boundary condition at the RF cavity surface:

$$k_c(\vec{n}\mathbf{grad}T) = P_s, \tag{2}$$

where $k_c = 391\frac{W}{m \cdot K}$ is the heat conductivity of copper, $\vec{n}$ is the unit normal vector to the cavity surface, $P_s$ is the RF loss density,

$$\int_s P_s dS = P_a, \tag{3}$$

and $P_a$ is the total average RF power, dissipated in the cavity.
We use an approximmative engineering approach by applying at the surface of the cooling channels the boundary condition:

$$k_c\frac{\partial T}{\partial n} = h_w(T - T_{ref}), \tag{4}$$

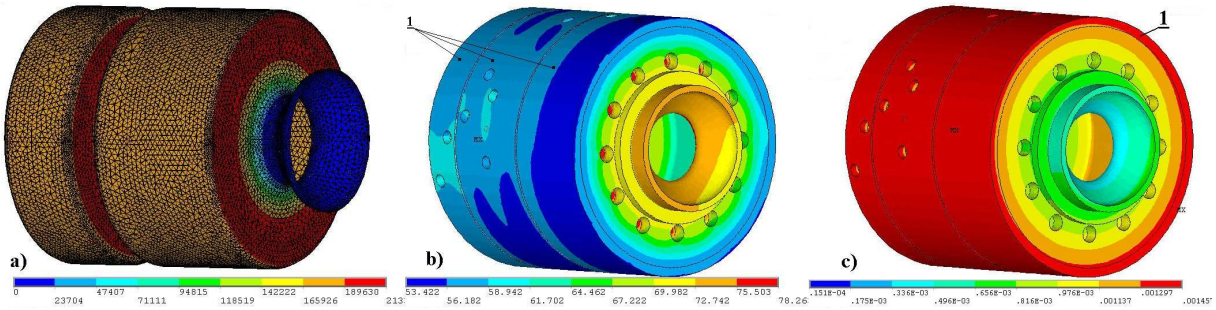


Figure 2.1: The typical distributions of RF losses at the cavity RF surface (a), temperature (b) and displacements (c) for RF Gun cavity. 1 - stainless steel jacket.

where $h_w, [\frac{W}{m^2 K}]$ is the heat exchange coefficient, $T_{ref}$ is some reference temperature, considered as a constant value at the channel surface. The value $h_w$ is an input parameter for simulations and should be determined from flow parameters of the coolant. Because all definitions of $h_w$ are approximated, we will apply definition, used in [2].

$$h_w = k_w \frac{Nu}{d_w}, \quad d_w = \frac{4A_p}{P_p}, \tag{5}$$

$$Nu = \frac{g}{8} \frac{(Re - 1000)Pr}{1 + 12.7\sqrt{\frac{g}{8}}(Pr^{\frac{2}{3}} - 1)}, \quad g = \frac{1}{(0.79ln(Re) - 1.64)^2}, \tag{6}$$

with

$$Re = \frac{V_{av} d_w \rho_w}{\eta_w}, \qquad Pr = \frac{\eta_w C_w}{k_w}, \qquad V_{av} = \frac{F_r}{A_p}, \tag{7}$$

where $Nu, Re, Pr$ are the Nusselt, Reynolds and Prandtl numbers for water flow, $d_w, A_p, P_p$ are the hydraulic diameter, area and perimeter of the cooling channel, $F_r, V_{av}$ are the flow rate ($[\frac{m^3}{sec}]$) and average flow velocity ($[\frac{m}{sec}]$) in the channel, $\rho_w = 987.2[\frac{kg}{m^3}]$, $k_w = 0.645[\frac{W}{m \cdot K}]$, $C_w = 4190[\frac{J}{kg \cdot K}]$, $\eta_w = 5.51 \cdot 10^{-4}[\frac{kg}{m \cdot sec}]$ are water density, heat conductivity, specific heat and dynamic viscosity, respectively. The values for water parameters $\rho_w, k_w, C_w$ and $\eta_w$ are chosen for a water temperature of $50C^o$, if it is not mentioned specially.

After the temperature distribution $T(\vec{r})$ is found, we define thermal elastic displacements $\vec{x}$ by solving the general equation for thermal expansion [3]:

$$\frac{3(1-\nu)}{1+\nu} \mathbf{grad\ div\vec{x}} - \frac{3(1-2\nu)}{2(1+\nu)} \mathbf{rot\ rot\vec{x}} = \alpha \mathbf{gradT}, \tag{8}$$

where $\alpha$, $\nu$ and $E_{el}$ are the linear expansion coefficient and Poisson ratio of the material. For copper these parameters are $\alpha_c = 1.66 \cdot 10^{-5} \frac{1}{K}$ and $\nu_c = 0.32$, respectively.
According to the perturbation theorem, the cavity frequency shift is:

$$\delta f = \frac{\pi f^2}{2QP_a} \int_S (\epsilon_0 E^2 - \mu_0 H^2)(\vec{x}\vec{n}) dS, \tag{9}$$

where $E, H$ are the electric and magnetic fields at the structure surface $S$, corresponding to the RF losses $P_a$, $Q, f$ are the quality factor and cavity frequency, calculated before.
As one can see from (1), (4) and (8), (9), we have, with respect to $P_a$, a linear problem.

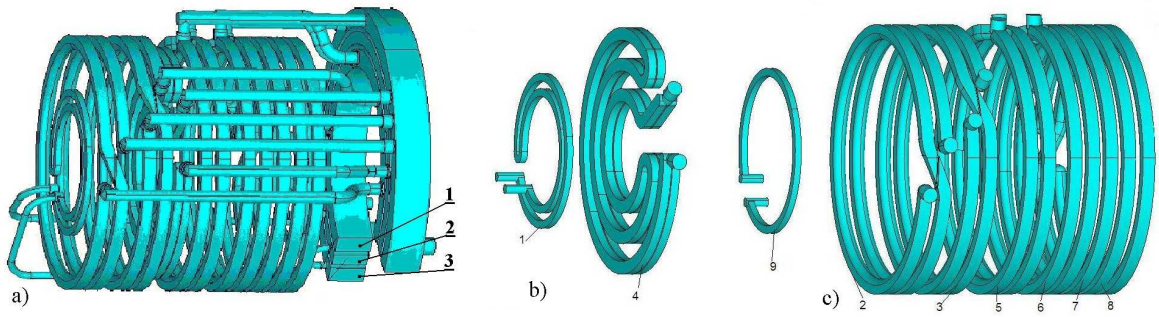


Figure 3.1: a) - Gun 3 cavity cooling circuit with distributing boxes, 1 - input box for cylindrical circuit, 2 - input box for radial circuit, 3 - common output box. b) - a radial sub circuit. c) - a cylindrical sub circuit. Channel numbering is shown in b) and c).

If we find the water flow distribution in the cooling channels, which results in a minimal frequency shift for one $P_a$ value, this distribution will provide also a minimal frequency shift for all other $P_a$ values.
The problem is also additive with respect to the $T_{ref}$ value. Of physical sense is a difference $T - T_{ref}$, which defines a frequency shift, assuming the initial frequency value being realized at the cavity reference temperature.
The cooling circuit of the Gun cavities has no symmetry. To avoid additional approximations, we solve the problem for the total cavity. Typical distributions of RF losses at the cavity RF surface, temperature and displacements distributions at the external surface are shown in Fig. 2.1a,b,c respectively.
The precision of the $\delta f$ calculation has been checked with a uniform cavity expansion. Assuming a uniform cavity material (copper), the average cavity heating of a temperature $\Delta T$ results in a uniform cavity expansion and frequency decreasing of:

$$\delta f = -f\alpha\Delta T. \tag{10}$$

For $\Delta T = 5C^o, \quad f = 1300MHz$ the frequency shift, defined from (10), is $107973Hz$, the numerically calculated value is $109974.2Hz$. The relative error of the numerical procedure is $\sim 1.85\%$. All DESY Gun cavities have in the design a stainless steel jacket, Fig. 2.1c. This jacket improves the cavity rigidity and decreases the radial cavity expansion. The cavity material is not uniform and equation (10) is not valid for frequency shift estimation for a uniform cavity uniform heating. Assuming the stainless steel parameters $\alpha_s = 1.0 \cdot 10^{-5}\frac{1}{K}$, $\nu_s = 0.27$ and Young module values for stainless steel $E_{els} = 2.06 \cdot 10^{11}\frac{N}{m^2}$ and for copper $E_{elc} = 1.17 \cdot 10^{11}\frac{N}{m^2}$, the numerically calculated frequency shift for the real Gun N3 design is $86319.1Hz$ for $\Delta T = 5C^o$, corresponding to $17264.8\frac{Hz}{C^o}$.

# 3 Gun 3 cooling circuit operation optimization

A Gun 3 cooling circuit is shown in Fig. 3.1a. It has two independent sub circuits with separat inputs and a common output. The first sub circuit, Fig. 3.1b, is intended for cooling of the radial cavity parts - cathode back wall, iris and front wall, the second one, Fig. 3.1c, is intended for cooling the cylindrical cavity wall. Each sub circuit has an input box with connecting tubes (outside the cavity) to the cooling channels, placed inside the cavity. Due

Table 3.1: Relative water flow distribution ($\cdot 10^3$) between channels in the Gun 3 cooling circuit and the channels cross-section area $S_{cch}, cm^2$. For channels conformity see Fig. 3.1b, Fig. 3.1c.

| Channel number | 1 | 2 | 3 | 4 | 5 | 6 | 7 | 8 | 9 |
|---|---|---|---|---|---|---|---|---|---|
| Radial circuit | 143 | | | 672 | | | | | 185 |
| Cylindrical circuit | | 134 | 155 | | 180 | 161 | 187 | 183 | |
| $S_{cch}$ | 0.3 | 1.1 | 1.1 | 1.3 | 1.1 | 1.1 | 1.1 | 1.1 | 0.3 |

to such circuit design, only a total flow rate is defined for each sub circuit - $Fl_1$ for the radial and $Fl_2$ for the cylindrical sub circuit.

## 3.1 Flow distribution in sub circuits

For the cooling simulations we have to know the flow rate in each channel. The problem of the flow distribution between separate channels in each sub circuit has been solved earlier and here only results are given.
The numbering of the cooling channels for the total Gun 3 cooling circuit is shown in Fig. 3.1b, Fig. 3.1c. The relative flow distribution between the channels is presented in Table 3.1. Assuming the same pressure drop at both sub circuits, the general flow distribution between the radial and the cylindrical sub circuit is 0.192/0.808, ensuring approximately equal water velocities in the channels of both sub circuits. As one can see from (5) - (7), even water velocity defines the heat exchange coefficient $h_w$ value and, through cavity temperature and displacements, the cavity frequency shift - the final value, essential for operating regime optimization. Below we will present the results of the frequency shift $\delta f$ calculations in a wide range of flow values $Fl_1$ and $Fl_2$ for both sub circuits. Generally speaking, the data, presented in Table 3.1, may be not quite correct if the maximal flow velocity in one sub circuit strongly differs from the maximal velocity in the second sub circuit. Such a strong difference will lead to pressure balance deterioration in the common output box. This case was not investigated, but such a situation is not interesting for practice - we have to use all cooling channels approximately at the same conditions.

## 3.2 Calculated cavity frequency shift.

To study the cavity frequency shift $\delta f$ for different flow rates $Fl_1$ and $Fl_2$, a set of simulations has been performed. For this purpose a special procedure of automatic ANSYS runs has been developed for thermal-stress simulations with variable values of $h_w$, storage of results and further $\delta f$ calculations.
The flow rate in the radial sub circuit $Fl_1$ was changed within the limits $(0.095 \div 0.95)\frac{l}{sec}$, divided into 10 uniform steps. For each value of $Fl_1$ the flow rate in the cylindrical sub circuit $Fl_2$ was changed within the limits $(0.33 \div 3.3)\frac{l}{sec}$, also uniformly divided into 10 steps. Totally 100 combinations of $Fl_1, Fl_2$ were considered. For each $Fl_1, Fl_2$ combination flow velocities in all channels, using the data from Table 3.1, were defined and values of $h_w$ calculated from (5) - (7). The limiting $Fl_1, Fl_2$ values, $0.95\frac{l}{sec}$ and $3.3\frac{l}{sec}$, respectively, were chosen from the condition of an averaged (over all channels in the sub circuit) flow velocity in each sub circuit of $5\frac{m}{sec}$ - higher than a practically safe value. Because in each sub circuit the flow velocities between the channels are not equal, for the limiting $Fl_1, Fl_2$ values there were channels (in each sub circuit) with a flow velocity of $> 5\frac{m}{sec}$.

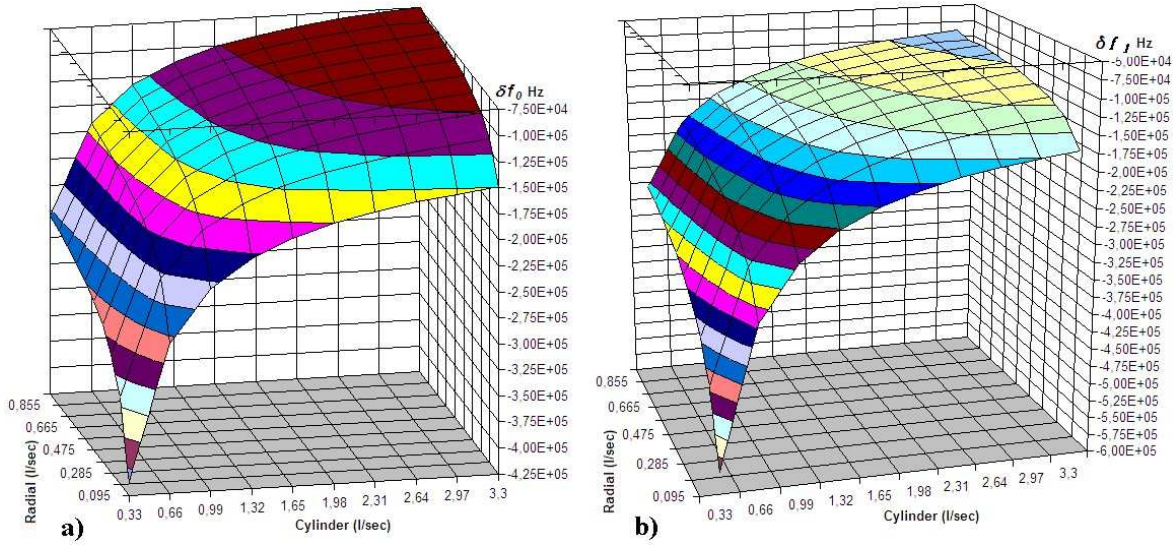


Figure 3.2: The surfaces of the cavity frequency shift $\delta f_0$ (a) and $\delta f_1$ in dependence on flow rates $Fl_1, Fl_2$ in the radial and cylindrical sub circuits, respectively, for $P_a = 31.787kW$, $T_{ref} = 48C^o = const$ (a) and $T_{ref} = \frac{T_{out}+T_{inc}}{2}$, b).

Simulations were performed assuming a constant $T_{ref} = 48C^o$ value and for an average RF power $P_a = 31.787kW$. As it was shown in Section 2, the problem is linear with respect to $P_a$ and $\delta f_0 = P_a \cdot F(Fl_1, Fl_2)$.

The resulting surface $\delta f_0 = P_a \cdot F(Fl_1, Fl_2)$ is shown in Fig. 3.2a. As one can see from Fig. 3.2a, it is monotonous with respect to $Fl_1$ and $Fl_2$ with positive partial derivatives $\frac{\partial(\delta f_0)}{\partial Fl_1} > 0$, $\frac{\partial(\delta f_0)}{\partial Fl_2} > 0$ in each surface point, reflecting the physical cavity behavior that every increase of the flow rate, regardless of the sub circuit, leads to a decrease of the frequency shift.

The assumption $T_{ref} = const$ is a zero approximation for the cavity $\delta f$ estimation. According to the physical sense, $T_{ref}$ in (4) is the bulk water temperature in the cooling channels. Going through the channel, the water heats up and the water temperature rises. We can measure the incoming and outgoing water temperature $T_{inc}$ and $T_{out}$. For each channel the difference $T_{out} - T_{inc}$ depends on both, the flow rate in this channel and the cooling ability of the other channels. In the framework of the engineering approach we cannot define these differences for each channel. For the whole cavity we can find the average temperature of the outgoing water, basing on energy conservation low:

$$T_{out} - T_{inc} = \frac{P_a}{C_w \rho_w (Fl_1 + Fl_2)}. \tag{11}$$

the next approximation considers the incoming water temperature $T_{inc}$ as a constant input value and usees as a new reference temperature for the cooling channels the averaged value $T_{ref} = \frac{T_{inc}+T_{out}}{2}$. Such a transformation means a uniform cavity heating by a temperature $\Delta T = \frac{T_{inc}-T_{out}}{2}$. In the cavity frequency shift estimation it is equivalent to the addition:

$$\delta f_{ad} = -\frac{P_a C_f}{2 C_w \rho_w (Fl_1 + Fl_2)}, \tag{12}$$

to each point of the initial surface $\delta f_0(Fl_1, Fl_2)$, shown in Fig. 3.2a, where $C_f = 17264.2\frac{Hz}{C^o}$ is the frequency sensitivity of the cavity with a stainless jacket, determined in Section 2.
As one can see from (12), the addition due to the increase of the average cavity temperature increasing is also proportional to $P_a$ and $\delta f_{ad}(Fl_1, Fl_2)$ is also monotonous with respect to $Fl_1$ and $Fl_2$ with positive partial derivatives $\frac{\partial(\delta f_{ad})}{\partial Fl_1} > 0, \frac{\partial(\delta f_{ad})}{\partial Fl_2} > 0$. This addition doesn't change the qualitative behavior of the resulting surface $\delta f_1(Fl_1, Fl_2) = \delta f_0(Fl_1, Fl_2) + \delta f_{ad}$, as shown in Fig. 3.2b as compared to the first surface $\delta f_0(Fl_1, Fl_2)$, shown in Fig. 3.2a.

## 3.3 Operating regime

During RF Gun cavity operation the cavity frequency should be constant, defined by the master generator. The RF power dissipation in the cavity leads to a frequency reduction. Before switching the RF power input on the temperature of the incoming water should be increased for $T_{inc1}$ and cavity should be heated with water to this temperature to adjust the cavity frequency at the operating value. To keep the frequency constant after RF power is switched on, the water temperature should be decreased to some new value $T_{inc2}$, which can be defined from:

$$T_{inc2} = T_{inc1} - \frac{\delta f_1}{C_f} = T_{inc1} - \frac{\delta f_0 + \delta f_{ad}}{C_f}. \tag{13}$$

The lower limit of $T_{inc2} \approx 30C^o$ is defined by parameters of the heat exchanger in the external (with respect to RF cavity) part of the cooling system. The upper value $T_{inc1}$ ($\approx 65C^o$) is also not infinite.
To dissipate the maximal RF power during cavity operation, one needs a minimal difference $T_{inc1} - T_{inc2}$ per unit of dissipated RF power, supposing optimal (and practical) values for the flow rates $Fl_1, Fl_2$ in the sub circuits. To find the optimal cooling regime, we have to find the minimal incoming temperature rate $T_{ri}(Fl_1, Fl_2)$:

$$T_{ri}(Fl_1, Fl_2) = \frac{T_{inc1} - T_{inc2}}{P_a} = \frac{\delta f_1}{C_f P_a}. \tag{14}$$

The maximal value of possible dissipated RF power $P_{amax}$ can be defined as:

$$P_{amax} = \frac{(T_{inc1} - T_{inc2})_{max}}{|T_{ri}(Fl_1, Fl_2)_{min}|}. \tag{15}$$

From (13) one can see that the minimal $T_{inc1} - T_{inc2}$ difference corresponds to the minimal $\delta f_1(Fl_1, Fl_2)$ and, correspondingly, to the minimal $\delta f_0(Fl_1, Fl_2)$.
From the monotonous behavior of the $\delta f_0(Fl_1, Fl_2)$ it follows that **the problem of optimal Gun 3 cavity cooling has no general solution - every increase of the flow**, regardless whether in the radial or cylindrical sub circuit, **leads to a decrease of the cavity frequency shift.** But we cannot increase the flow rates in the cooling sub circuits infinitely - there are some technical limitations.

## 3.4 Limitations to the Gun 3 cavity cooling regime

The first limitation, which can be considered, is the limited pumping power, $Fl_1 + Fl_2 \leq Fl_0 = const$. In the Gun 3 cooling circuit design the radial and cylindrical sub circuits are strongly unequal in admission. In this case the range of flow rates $Fl_1, Fl_2$ consideration is

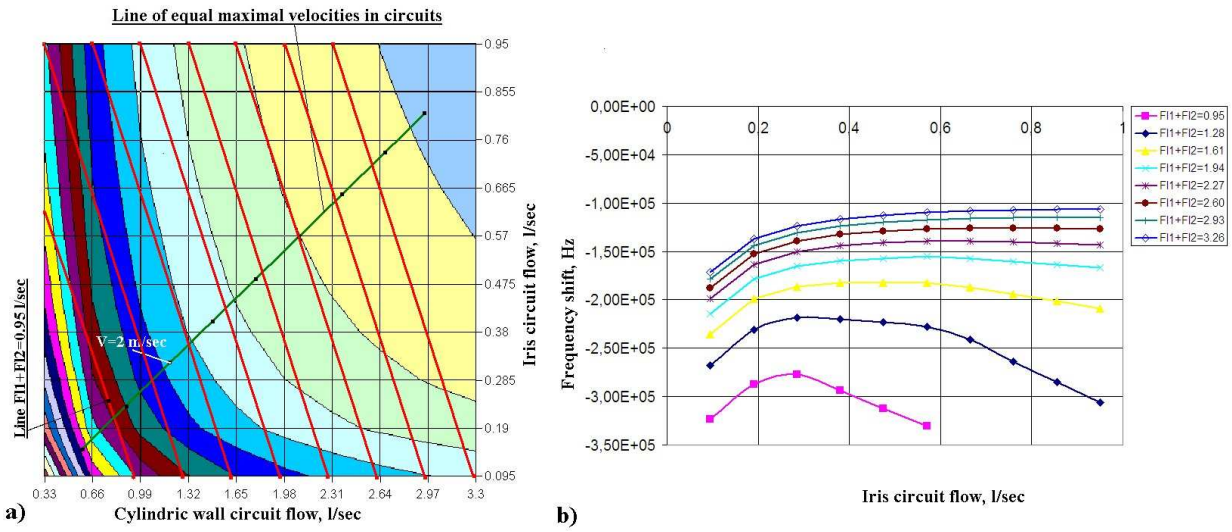


Figure 3.3: The isolines of $\delta f_1(Fl_1, Fl_2)$ surface a) and the plots of $\delta f_1(Fl_1, Fl_2)$ along the lines $Fl_1 + Fl_2 = const \frac{l}{sec}$, b). See explanations in the text.

limited to the sub circuit of the lowest submission - the radial sub circuit.
In Fig. 3.3a the isolines for the surface $\delta f_1(Fl_1, Fl_2)$ are shown for flow rate changes $0.095\frac{l}{sec} \leq Fl_1 \leq 0.95\frac{l}{sec}$, $0.33\frac{l}{sec} \leq Fl_1 \leq 3.3\frac{l}{sec}$ and the lines $Fl_1 + Fl_2 = Fl_0 = const$ for different $Fl_0$ values. These lines $Fl_1 + Fl_2 = Fl_0 = const$ are represented with red lines in Fig. 3.3a for $Fl_0 = 0.95; 1.28; 1.61; 1.94; 2.27; 2.60, 2.93; 3.26\frac{l}{sec}$. In Fig. 3.3b the plots of the $\delta f_1(Fl_1, Fl_2)$ dependence is shown along these lines $Fl_1 + Fl_2 = Fl_0 = const$ for the $Fl_0$ values, mentioned above.
As one can conclude from the surface $\delta f_1(Fl_1, Fl_2)$ behavior, (see Fig. 3.2b, Fig. 3.3a), the dependence of $\delta f_1(Fl_1, Fl_2)$ should have an extremum along the line $Fl_1 + Fl_2 = const$ for low values of $Fl_0$. For $Fl_0 = 0.95\frac{l}{sec}$ and $Fl_0 = 1.28\frac{l}{sec}$ one can see an evident extremum in the plots in Fig. 3.3b - for flow rates $Fl_1 \approx 0.3\frac{l}{sec}$ the cavity frequency shift is minimal under these limitations. For larger $Fl_0$ values the plots $\delta f_1(Fl_1, Fl_2)$ become smoother and for $Fl_0 \geq 2.6\frac{l}{sec}$ there is no extremum. The limitation $Fl_1 + Fl_2 = Fl_0 = const$ is not interesting for practical Gun 3 operation. A flow redistribution between the two sub circuits can lead to a relatively minimal $\delta f_1(Fl_1, Fl_2)$ at a low total flow $Fl_0$ but these values are larger than for a larger total flow. For a high total flow redistribution is not possible, because the limit from flow velocities in the radial sub circuit cooling channels becomes earlier, than the minimal frequency shift value.
For a well designed sub circuit the flow velocities should be approximately equal, but a velocity spread exists practically for all time. For the Gun 3 cooling circuit a maximal flow velocity in the radial sub circuit has channel $N9$, see Fig. 3.1, and in the cylindrical sub circuit - channel $N7$.The flow velocity in the cooling channel is limited by cavity life time reasons - at a very high flow velocity material erosion can occur due to cavitation in turbulent flow, vibrations and so on.
Let us suppose the cooling regime when the maximal flow velocities in channels $N9$ and $N7$ for Gun 3 are equal. At first, it would lead to similar conditions for material life time. Also it means a maximal flow rate a for sub circuit with respect to a maximal flow velocity. As one can see from Fig. 3.2, Section 3.2, for a minimal frequency shift there should be a maximal

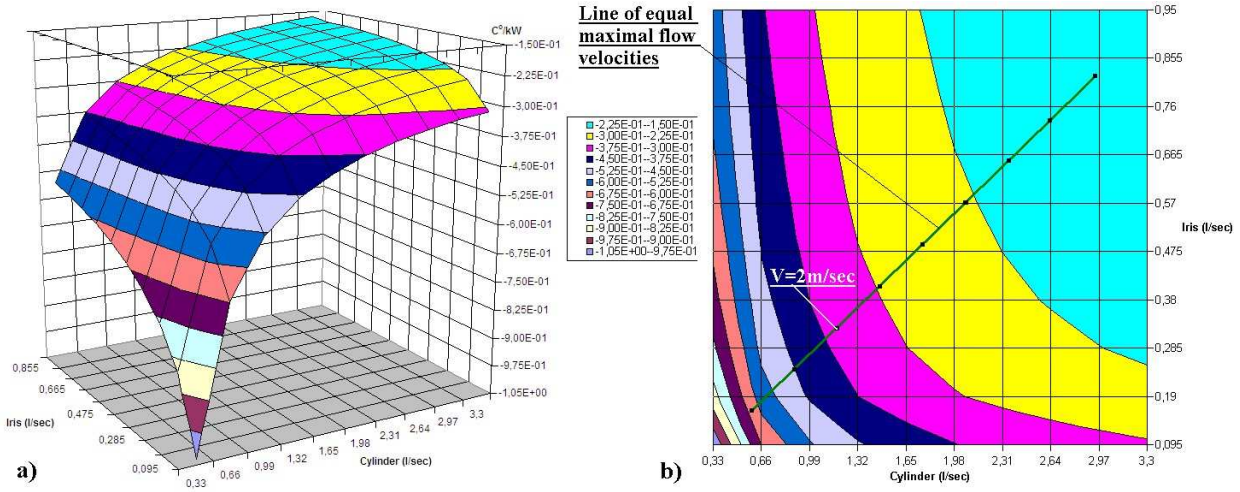


Figure 3.4: The surface of incoming water temperature rate $T_{ri}(Fl_1, Fl_2)$ in dependence on the maximal velocity in channels $N7, N9$ a), and isolines of this surface,b).

flow in both sub circuits. This cooling regime is reflected in Fig. 3.3a with a green line. The black dots at the green line correspond to flow velocities of $(1.0 \div 5.0)\frac{m}{sec}$ in channels $N7$ and $N9$. The flow velocity $2.0\frac{m}{sec}$ in channels $N7$ and $N9$ corresponds to $Fl_1 = 1.168\frac{m^3}{h}$ in the radial sub circuit and $Fl_2 = 4.236\frac{m^3}{h}$ in the cylindrical one. To realize such a cooling regime concept, we have to keep the flow rates ratio $\frac{Fl_1}{Fl_2} = 0.276$. It **differs from the flow ratio** $\frac{Fl_1}{Fl_2} = 0.238$, which **corresponds to the same pressure drop at the sub circuits**, see Section 3.1.

The surface of incoming water temperature rate $T_{ri}(Fl_1, Fl_2)$, (14), in dependence to the flow rates $Fl_1$ and $Fl_2$ through the cavity together with isolines of this surface are shown in Fig. 3.4a,b respectively.

Considering the surfaces behavior for the cavity frequency shift $\delta f_1(Fl_1, Fl_2)$, Fig. 3.2b, and the incoming water temperature rate $T_{ri}(Fl_1, Fl_2)$, Fig. 3.4a, or $\delta f_1(Fl_1, Fl_2)$ and $T_{ri}(Fl_1, Fl_2)$ isolines, Fig. 3.3a and Fig. 3.4b, respectively, one can see fast changes for small flow values and saturation the in changes for large flows. Large increase of the flow velocity, more than $(3.0 \div 3.5)\frac{m}{sec}$, is not effective in cavity parameters change. The usual flow velocity $V = 2\frac{m}{sec}$ corresponds to flow values, which provide moderate parameters change - not so big as compared to low flow velocity and not so small as for high one.

Assuming the maximal range of incoming water temperature change $T_{inc2} - T_{inc1} = 35C^o$, we can estimate from (15) and the obtained $T_{ri}(Fl_1, Fl_2)$ values, Fig. 3.4b, the maximal dissipated RF power for the given $Fl_1$ and $Fl_2$ values. The surface of maximal dissipated RF power and isolines of this surface are shown in Fig. 3.5a,b, respectively, for the Gun 3 cooling circuit in dependence on the flow rates $Fl_1$ and $Fl_2$. The results, presented in Fig. 3.5b show, that from the point of cavity frequency shift control, which is reflected in estimations (13) - (15), a high RF power can be dissipated in Gun 3 cavity. Even for the usual value of the maximal flow velocity in channels $N7$ and $N9$ $V = 2\frac{m}{sec}$, an RF power $\sim (90 \div 105)kW$ can be dissipated. For a maximal flow velocity $V = 5\frac{m}{sec}$ the tolerable RF power is $\approx 195kW$, see Fig. 3.5b. The limitation for the maximal RF power for Gun 3 comes from the temperature values.

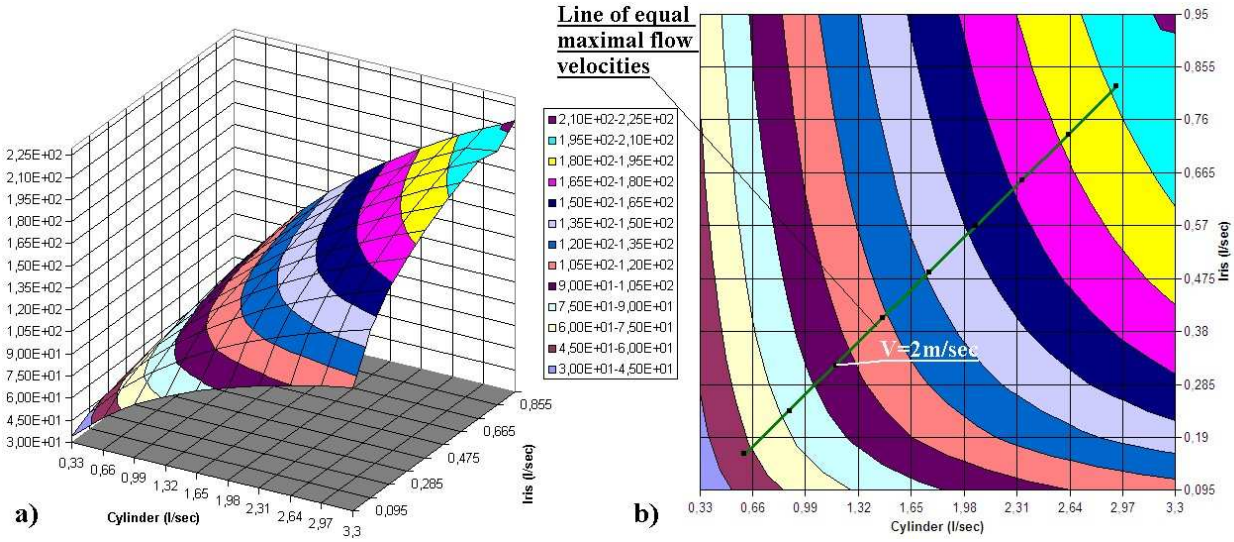


Figure 3.5: The surface of maximal dissipated RF power in Gun 3 cavity a) and isolines of this surface - b) in dependence on water flow rates in the radial and cylindrical sub circuits $Fl_1$ and $Fl_2$.

All DESY Gun cavities have a temperature sensor, placed in the iris. The surface of the iris temperature rise (with respect to the incoming water temperature $T_{inc}$) is shown in Fig. 3.6a and isolines of this temperature rise - in Fig. 3.6b in dependence on the water flows $Fl_1$ and $Fl_2$. The temperature inside the iris depends mainly on the flow rate in the radial sub circuit $Fl_1$. From Fig. 3.6b one can see a fast iris temperature decrease with increasing $Fl_1$ for small $Fl_1$ values (flow velocity in channel $N9 \leq 1.5\frac{m}{sec}$) and saturation at a high flow velocity of $\geq 4\frac{m}{sec}$.

Another important parameter is the maximal temperature at the cavity surface. The surface of the maximal temperature rise $\delta T_{max}$ (with respect to the incoming water temperature $T_{inc}$) is shown in Fig. 3.6c and isolines of this temperature rise - in Fig. 3.6d in dependence on water flows $Fl_1$ and $Fl_2$. We see the same qualitative behavior - fast change (decreasing) of maximal surface temperature for small flow rates in the sub circuits and saturation at large rates, which correspond to high flow velocities in the channels. The maximal temperature in Gun 3 at the cavity surface is invariably higher than the iris temperature. The values of temperature rise both in the iris and at the cavity surface **are presented for a dissipated RF power** $P_a = 31.787kW$**.** From the results, presented in Fig. 3.6 one can see tolerable temperature values both for the iris and the cavity surface. Estimating the maximal dissipated RF power from the point of view of cavity frequency shift compensation, one has to estimate also new temperature values, normalizing the results in Fig. 3.6 on the new RF power value, by using problem linearity with respect to dissipated RF power. For the dissipated RF power of $\sim 95kW$ the maximal surface temperature, as one can conclude from Fig. 3d, will be $\approx 100C^o$ higher than the incoming water temperature and can be $\approx 140C^o$. A stable operation of the cavity with such high surface temperature is not evident from the viewpoint of extensive outgasing.

**For the Gun 3 cavity the maximal possible dissipated RF power is limited by the maximal temperature at the cavity surface.**

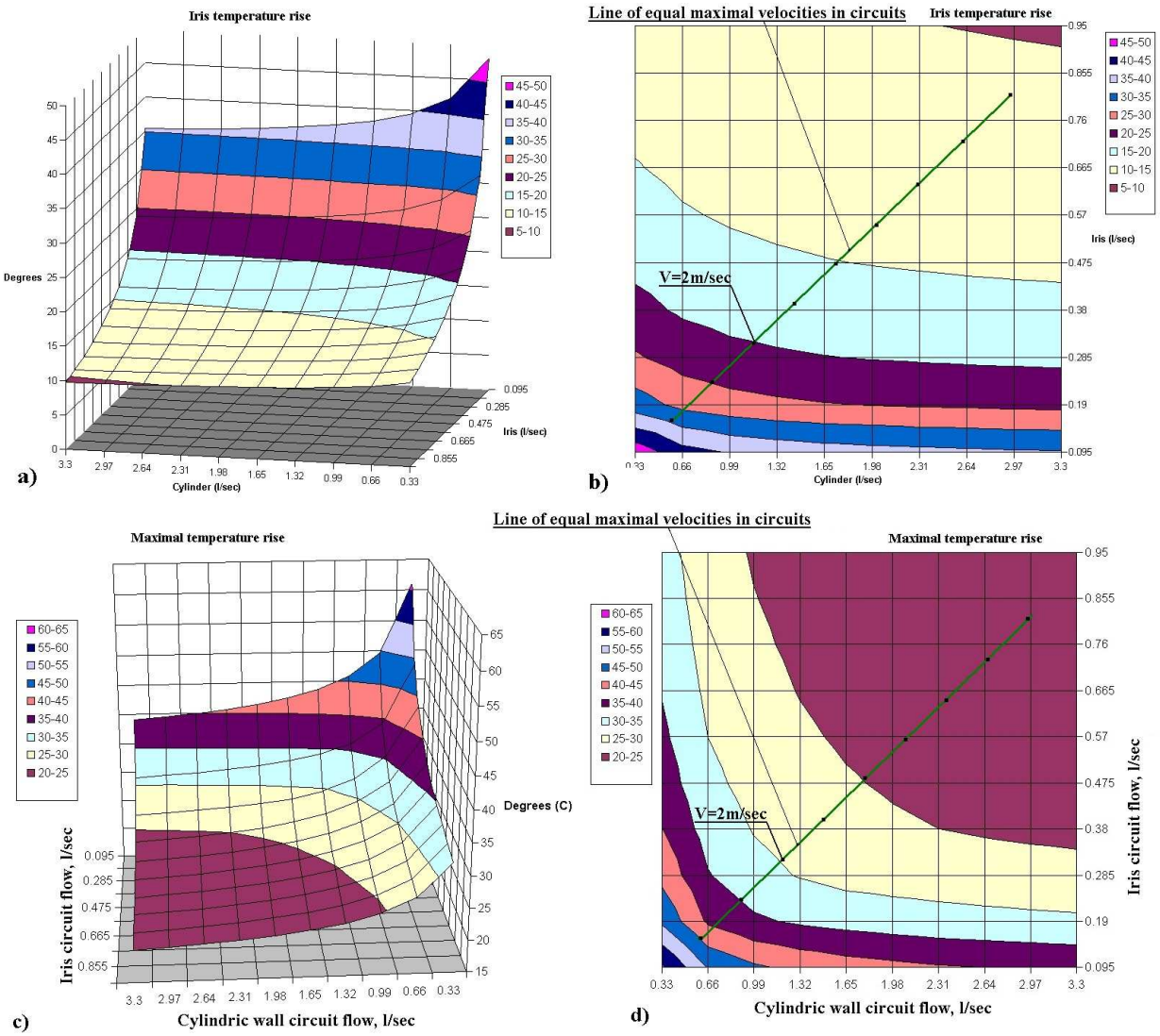


Figure 3.6: The surface of the iris temperature rise (with respect to $T_{inc}$) a) and isolines of this temperature rise, b). The surface of the maximal temperature rise $\delta T_{max}$ at the cavity surface (with respect to $T_{inc}$) is c) and isolines of this temperature rise - d) in dependence on water flows in the radial and cylindrical sub circuits $Fl_1$ and $Fl_2$. $P_a = 31.787kW$, $T_{ref} = \frac{T_{inc}+T_{out}}{2}$.

## 3.5 Comparison with experiments

In our simulations we have to do several assumptions, which can change the quantity for calculated parameters.
We use an engineering approach for the cooling simulations with input parameter $h_w$. To estimate the cooling ability, we need the frequency shift calculation. To apply a conjugated approach for the heat exchange problem we have to consider the total cavity. To solve the problem with a reasonable precision, we would, however need at least one order of magnitude more in computing power.
We assume a uniform average cavity heating due to the water heating in the cooling channels. It partially compensates the disadvantage of the engineering approach. A nonuniform cavity heating cannot be simulated with such assumptions.
We assume constant material parameters and neglect the parameters dependence on the temperature. This may change the results of the simulations for poor cooling, when the cavity temperature rise is essential. For a real operational cooling with a temperature rise of $\sim 30C^o$ this effect gives only second order additions, especially on the background of the previously discussed assumptions.
We use the material parameters as published in handbooks. This point may be essential, taking into account the DESY Gun design with stainless jackets. For the main cavity body high quality OFE copper is used, and parameters for this material are known to be enough reliable, with a relatively narrow spread. In our estimations we use frequently the value $C_f$ (Eq. 12) for the cavity expansion with uniform heating, which depends on the Young modulus ratio for copper and stainless steel $\frac{E_{els}}{E_{elc}}$. The dependence $C_f$ on the $\frac{E_{els}}{E_{elc}}$ ratio is shown in Fig. 3.7 and exhibits a reduction of $C_f$ with increasing $\frac{E_{els}}{E_{elc}}$. The increased $\frac{E_{els}}{E_{elc}}$ ratio means a more rigid jacket, which restricts the cavity expansion in radial direction and redistributes displacements to the longitudinal direction. The cavity operating mode can be specified as $TM_{011}$. For such a mode the cavity frequency is much more sensitive to radial than to longitudinal surface displacements.
The assumptions and uncertainties, discussed above, do not change the qualitative behavior of the results and conclusions. It can effect the quantities of the calculated parameters. To make the estimations of the maximal dissipated RF power more confident a comparison with experimental results for Gun 3 cavity is required.
Some experiments have been performed with the operating Gun 3.2 cavity at the PITZ facility. Two points with different flow velocities were investigated. In experiments we cannot fix the cavity resonant frequency without RF power and measurements were performed for each cooling regime with two levels of dissipated RF power - as low as possible and as high as possible for stable operation. The operating RF regime was with an RF pulse length of $400\mu s$ and a repetition rate of $10Hz$. The two cooling regimes, investigated in measurements correspond to maximal flow velocities $V = 1\frac{m}{sec}$ and $V = 2\frac{m}{sec}$ in channels $N7$, $N9$. These are two points at the line of equal maximal flow velocities, shown in Fig. 3.3a, Fig. 3.4b, Fig. 3.5b and Fig. 3.6b,d. The experimental data are given below.
Point 1. $Fl_1 = 0.58\frac{m^3}{h}, Fl_2 = 2.10\frac{m^3}{h}, P_a = 4.22kW, T_{inc} = 67.02C^o, T_{out} = 68.4C^o$.
Point 2. $Fl_1 = 0.58\frac{m^3}{h}, Fl_2 = 2.10\frac{m^3}{h}, P_a = 20.8kW, T_{inc} = 56.1C^o, T_{out} = 63.8C^o$.
Point 3. $Fl_1 = 1.15\frac{m^3}{h}, Fl_2 = 4.20\frac{m^3}{h}, P_a = 2.136kW, T_{inc} = 68.64C^o, T_{out} = 68.84C^o$.
Point 4. $Fl_1 = 1.15\frac{m^3}{h}, Fl_2 = 4.20\frac{m^3}{h}, P_a = 20.096kW, T_{inc} = 60.88C^o, T_{out} = 64.41C^o$.
From point 1 and point 2, point 3 and point 4 we directly obtain the incoming water temperature rate $T_{ri}(Fl_1, Fl_2)$ for flow velocities $V = 1\frac{m}{sec}$ and $V = 2\frac{m}{sec}$. These are

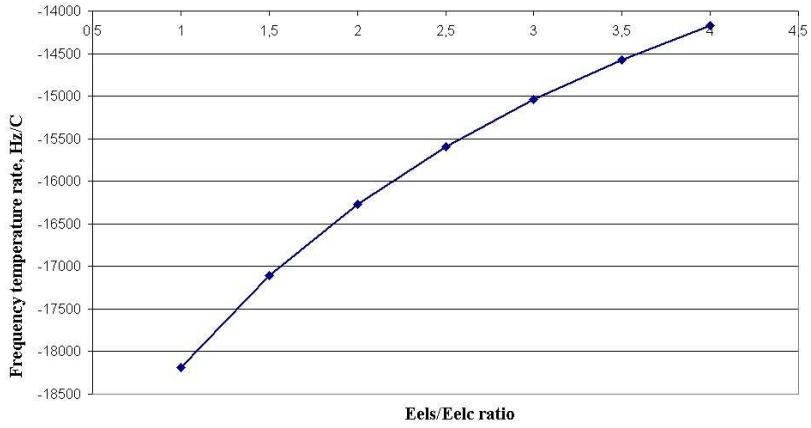


Figure 3.7: Calculated dependence of the frequency temperature rate $C_f$ on the Young module ratio $\frac{E_{els}}{E_{elc}}$ of stainless steel ($E_{els}$) and copper ($E_{elc}$).

$T_{ri}(0.58, 2.10) = 0.658\frac{C^o}{kW}$ for $V = 1\frac{m}{sec}$ and $T_{ri}(1.15, 4.20) = 0.389\frac{C^o}{kW}$ for $V = 2\frac{m}{sec}$. The calculated values are $T_{ri}(0.58, 2.10) = 0.642\frac{C^o}{kW}$ and $T_{ri}(1.15, 4.20) = 0.362\frac{C^o}{kW}$, respectively. The relative difference between the calculated and withdrawn values is $\approx 3\%$ and can be explained well by the precision of both the measurements and the calculations.
For the calculated and the measured iris temperature rise the coincidence is not so good - the calculated values are $\approx 20\%$ lower than the measured values. The reason has not been revealed yet.
Based on the results of the comparison we can conclude that the value of the maximal dissipated RF power, calculated from the requirements of cavity frequency shift control, is quite reliable. For the RF power limitation from the cavity temperature rise we should take into account a temperature under estimation in the simulations.
Considering the cooling ability of the Gun 3 circuit and the cavity parameter behavior for different flow rates in the radial and cylindrical sub circuits, one can conclude that in general the cooling ability (and maximal value of dissipated RF power) of the Gun 3 cavity is limited only by a reasonably safe value of the maximal surface temperature and flow velocity in the cooling channels. As reasonable solution **we can recommend the equal maximal flow velocities in both sub circuits**. For low flow rates and low related flow velocities the cooling ability has a big reserve and we see a sufficient parameter change with increase of the flow rate. But, this is a boundary of reasonability - for high flow velocities we see a saturation in the parameter. We have no rigid limitation for an upper flow velocity. But, as consideration shows, velocities above $\sim (3 \div 4)\frac{m}{sec}$ don't lead to significant improvements in the cooling ability and maximal dissipated RF power.

# 4 RF Gun 2 cooling circuit operation study

The Gun 2 cooling circuit has a very similar geometry as the circuit of Gun 3 cavity and also has two independent sub circuits for cooling of the radial and cylindrical walls. The Gun 2 sub circuit for the cylindrical wall cooling has, in contrast to that of Gun 3, all channels with only one turn. The total number of channels in the Gun 2 cylindrical sub circuit is 11, instead of 6 (five two turn and one single turn) channels in the Gun 3 sub circuit. Also the

Table 4.1: Relative water flow distribution ($\cdot 10^3$) between the channels in Gun 2 cooling circuit and the channels cross-section area $S_{cch}, cm^2$.

| Ch. N | 1 | 2 | 3 | 4 | 5 | 6 | 7 | 8 | 9 | 10 | 11 | 12 | 13 | 14 |
|---|---|---|---|---|---|---|---|---|---|---|---|---|---|---|
| Rad. | 171 | | | | | 628 | | | | | | | | 201 |
| Cyl. | | 166 | 93 | 56 | 69 | | 74 | 78 | 82 | 94 | 88 | 99 | 102 | |
| $S_{cch}$ | 0.3 | 1.1 | 1.1 | 1.1 | 1.1 | 1.3 | 1.1 | 1.1 | 1.1 | 1.1 | 1.1 | 1.1 | 1.1 | 0.3 |

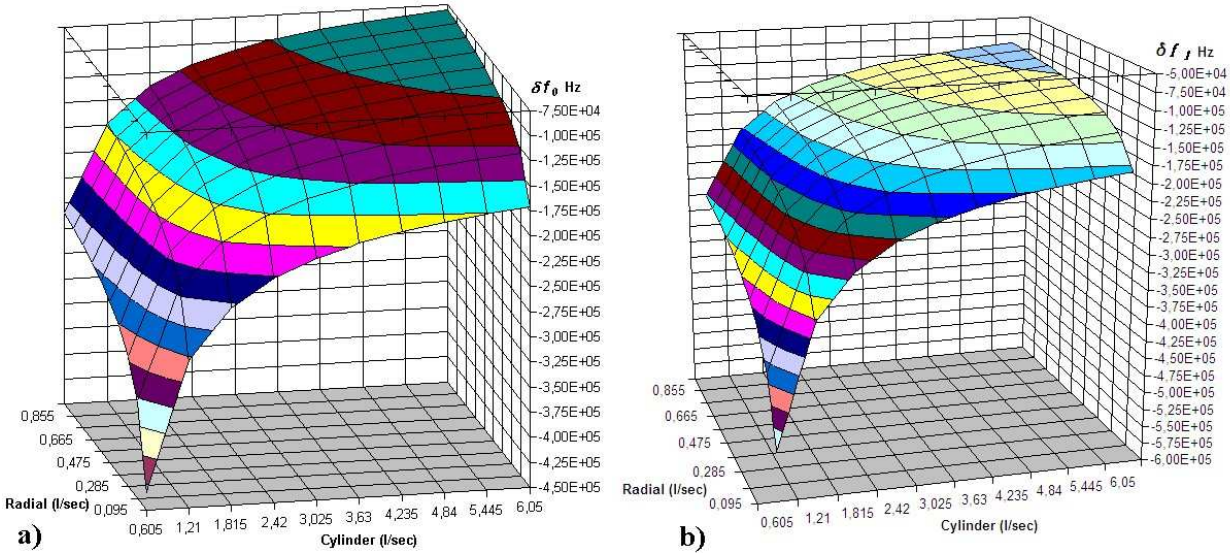


Figure 4.1: The surfaces of the Gun 2 cavity frequency shift $\delta f_0$ (a) and $\delta f_1$ in dependence on flow rates $Fl_1, Fl_2$ in radial and cylindrical sub circuits, respectively, for $P_a = 31.787kW$, $T_{ref} = 48C^o$ (a) and $T_{ref} = \frac{T_{out}+T_{inc}}{2}$, b).

position of tube connection between the channels and the distributing box is different for both sub circuits, as compared to Gun3 cooling circuit design.

The study of the Gun 2 cooling regime has been performed in the same way as for that of Gun 3. In this Section we will present and discuss just the final results and compare them with the equivalent results for the Gun 3 cavity.

The problem of the flow distribution between the Gun 2 sub circuits was solved before and the results are presented in Table 4.1.

Due to the large number of channels, the Gun 2 cylindrical sub circuit has a smaller hydraulic resistance. Assuming the same pressure drop at the sub circuits, the general flow distribution between the radial and cylindrical sub circuit is 0.118/0.882. Channel number 2 in the cylindrical sub circuit differs strongly in the relative water flow with respect to the other channels in this group. The connecting input tube of this channel is placed opposite of the input tube of the distributing box and we have an enlarged direct flow into this channel. To provide the same flow velocities in the Gun 2 cylindrical sub circuit, more water is required and the range of flow values $Fl_2$ for the cavity frequency shift calculations was extended from $Fl_2 = 3.3\frac{l}{sec}$ for the Gun 3 cavity to $Fl_2 = 6.05\frac{l}{sec} = \frac{3.3 \cdot 11}{6}\frac{l}{sec}$ to reach the same average flow velocity $V = 5\frac{m}{sec}$ over all channels. Simulations of the cavity frequency shifts $\delta f_0(Fl_1, Fl_2)$ and $\delta f_1(Fl_1, Fl_2)$ were done with a similar procedure as for the Gun 3 cavity, with the same dissipated RF power $P_a = 31.787kW$. The calculated results are presented in Fig. 4.1 with

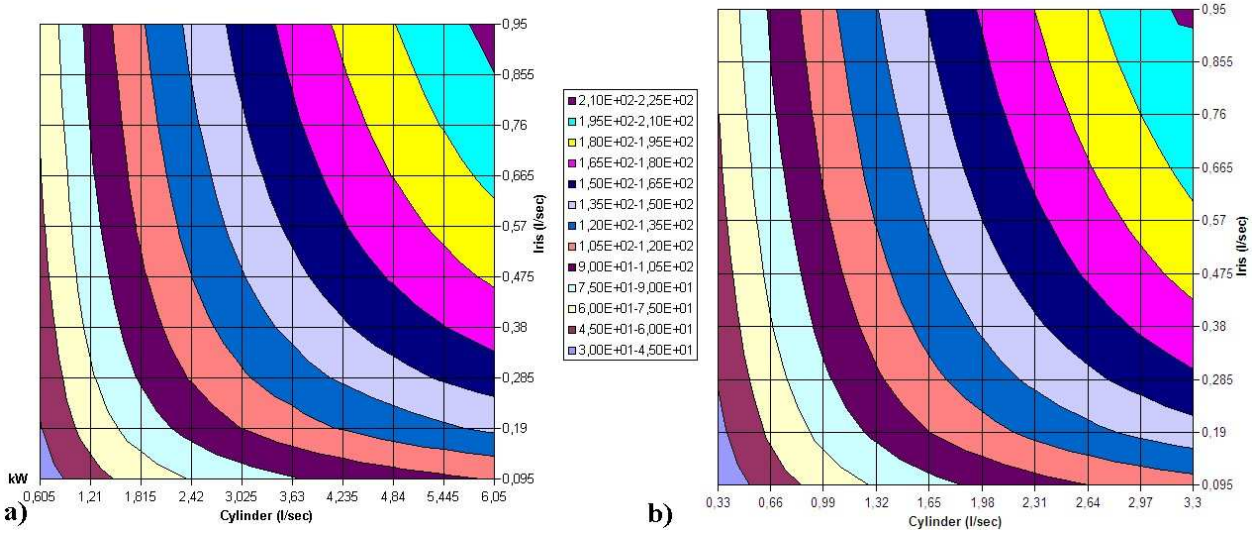


Figure 4.2: The isolines of the maximal dissipated RF power in Gun 2 cavity a) and Gun 3 one b) in dependence on flow rates $Fl_1, Fl_2$ in radial and cylindrical sub circuits, respectively.

the surface $\delta f_0(Fl_1, Fl_2)$ (Fig. 4.1a) and with the surface $\delta f_1(Fl_1, Fl_2)$ (Fig. 4.1b).
Comparing the surfaces in Fig. 4.1 for the Gun 2 cavity with the equivalent results for Gun 3 in Fig. 3.2, one can see the same qualitative behavior. All the conclusions, made for the Gun 3 cavity cooling circuit are valid for that of Gun 2, with a correction of the total flow value. Due to the similar cavity design, the values of the cavity frequency shifts $\delta f_0(Fl_1, Fl_2)$, calculated with the assumption $T_{ref} = const = 48C^o$, are practically the same for both cavities. With the increased water flow in the cylindrical sub circuit, the Gun 2 cavity has a smaller total cavity frequency shift $\delta f_1(Fl_1, Fl_2)$, because the addition $\delta f_{ad}$ (12) is smaller for the same RF power.
Other results for the Gun 2 cavity, such as the incoming water temperature rate $T_{ri}(Fl_1, Fl_2)$ (14), the temperature rise at the iris and the maximal temperature at the cavity RF surface, are practically the same, as shown in Fig. 3.4 and Fig. 3.6 for the Gun 3 cavity, if one takes into account the enlarged ($\frac{11}{6}$) flow rate $Fl_2$ for the Gun 2 cylindrical sub circuit. With this increased $Fl_2$ we provide approximately equal values for the heat exchange coefficient at the surface of the cooling channels in the cylindrical sub circuits both of the Gun 3 and the Gun 2 cavities and the results must be very similar.
The isolines of maximal dissipated RF power are shown for the Gun 2 cavity in Fig. 4.2a, and for the Gun 3 cavity in Fig. 4.2b. The maximal dissipated RF power is the same for both cavities and maximal $P_a$ value for the Gun 2 cavity is also restricted by the maximal surface temperature.

# 5 RF Gun 4 cooling circuit study.

In contrast to Gun 2 and Gun 3, the Gun 4 cooling circuit, shown in Fig. 5.1, consists of 14 independent channels. Even in simulations, we cannot consider directly all different combinations of water flow in all 14 channels. The task to have a maximal dissipated RF

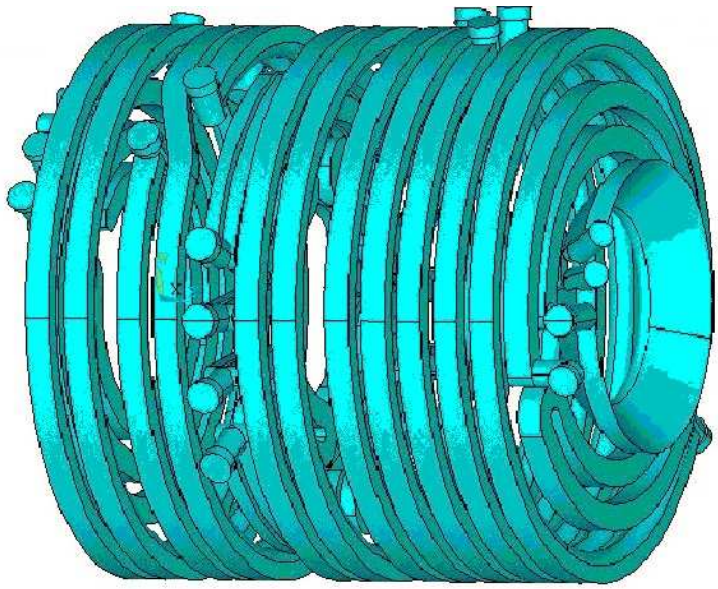

Figure 5.1: The Gun 4 cooling circuit.

Table 5.1: The channels cross section areas $S_{cch}, cm^2$ in the Gun 4 cooling circuit.

| $Ch.N$ | 1 | 2 | 3 | 4 | 5 | 6 | 7 | 8 | 9 | 10 | 11 |
|---|---|---|---|---|---|---|---|---|---|---|---|
| $S_{cch}$ | 1.0 | 1.0 | 1.1 | 1.1 | 4x1.2 | 1.1 | 1.1 | 1.1 | 1.1 | 1.0 | 1.35 |

power at a defined total flow rate is equivalent to the task to have a minimal cavity frequency shift. We cannot find an optimal combination of flow rates in the channels which minimizes the frequency shift, but we can show a way toward this combination, by investigating the cavity frequency sensitivity with respect to flow deviations the in different channels. As it was shown in Section 2, the problem under consideration is linear with respect to $P_a$. Because the Gun 4 cavity is developed for a higher RF power operation, all numerical results, presented for this cavity, are calculated for $P_a = 60kW$.
Another attractive feature of the Gun 4 circuit design is the possibility to change the frequencies of the individual cavity cells and hereby to change the electric field distribution between the cells in the cavity.

## 5.1 Frequency sensitivity to water flow deviations in the channels

Suppose we have a reference operating regime for the Gun 4 cooling circuit with equal flow velocities $V_0 = 2\frac{m}{sec}$ in all the channels and a corresponding cavity frequency shift $\delta f_0$. Let us investigate the sensitivity of the cavity frequency shift to the flow rate changes in the channels. For this purpose we will change the flow velocity in one channel and keep the reference flow velocity $V_0 = 2\frac{m}{sec}$ in all other channels constant. The measurable quantity is the flow rate through the channel. To estimate the velocity, the areas of the channel cross sections are given in Table 5.1. The numbering of the channels start at the cathode and goes toward the RF coupler. The four iris channels are considered as a single channel - number $N = 5$ in Table 5.1.

By changing the flow rate in one channel, we provide a local temperature change in the

Table 5.2: The cavity frequency shift sensitivity $\delta f_2 - \delta f_0, kHz$ to the flow velocity deviations in cooling channels. Reference flow velocity $V_0 = 2.0\frac{m}{sec}, P_a = 60kW$.

| **Channel N** | $V = 1.0\frac{m}{sec}$ | $V = 1.5\frac{m}{sec}$ | $V = 2.0\frac{m}{sec}$ | $V = 2.5\frac{m}{sec}$ | $V = 3.0\frac{m}{sec}$ |
|---|---|---|---|---|---|
| 1 | -8.94 | -3.51 | 0.0 | 2.52 | 4.44 |
| 2 | 2.21 | 0.94 | 0.0 | -0.71 | -1.29 |
| 3 | -10.24 | -3.88 | 0.0 | 2.65 | 4.59 |
| 4 | -13.70 | -5.34 | 0.0 | 3.78 | 6.63 |
| 5 iris | -49.72 | -17.95 | 0.0 | 11.79 | 20.23 |
| 6 | -15.37 | -5.98 | 0.0 | 4.22 | 7.39 |
| 7 | -25.70 | -9.85 | 0.0 | 6.80 | 11.82 |
| 8 | -6.05 | -2.62 | 0.0 | 2.10 | 3.82 |
| 9 | -6.35 | -2.54 | 0.0 | 1.84 | 3.24 |
| 10 | -1.93 | -0.84 | 0.0 | 0.69 | 1.28 |
| 11 | -2.31 | -1.00 | 0.0 | 0.82 | 1.49 |

vicinity of this channel and a related change in cavity deformation. As a result, we find another value of the cavity frequency shift $\delta f_2$. For us the difference $df = \delta f_2 - \delta f_0$ is interesting. Because there are no preliminary indications for a linearity or another $df(V)$ dependence, the $df$ values for each channel were calculated for flow velocities $V = (1.0 \div 3.0)\frac{m}{sec}$ with a step of $0.5\frac{m}{sec}$. The calculated $df$ values are presented in Table 5.2 and a selection is plotted in Fig. 5.2.

As one can see, the largest influence on the cavity operating frequency has the flow velocity in the iris channels. The maximal electric field value at the cavity surface is reached at the iris nose. The iris cooling deviations lead to a relatively small change of the inner iris diameter, but, due to the field distribution, it leads to a larger frequency deviation. The flow velocity deviations in channels $N7$ and $N6$, placed near the iris for the second cell cooling also have a relatively strong influence on the operating frequency, see Fig. 5.2. Flow deviations in the other channels have less influence, as compared to channel $N6$ and the plots are not shown in Fig. 5.2. Decreasing the flow in all channels, except channel $N2$, leads to a decreasing of operating frequency. The unusual influence of the flow deviations in channel $N2$ has no evident explanations - it is a result of simulations, which take into account both the non uniform RF loss distribution and the real 3D cavity design.

As one can see from Fig. 5.2, and it was also seen in the Gun 3 cooling circuit study, the influence of flow deviations on the operating frequency is non symmetric - a flow reduction provides a larger frequency deviation as compared to the same relative flow increase.

To realize the minimal cavity frequency shift during operation, one should provide a larger flow velocity in the channels with a large influence on the operating frequency - the iris channels and channels $N7$ and $N6$. This can be done at the expense of a flow reduction in the other channels - $N2, N10, N11, N8, N9$.

## 5.2 Field distribution change by flow control

The RF Gun cavity consists of a pair of coupled cells. In such a system the individual cells $TM_{010}$ modes originate two cavity modes. The operating cavity mode, with a higher frequency, is of $\pi$-type. A typical electric field distribution along the cavity axis is shown in

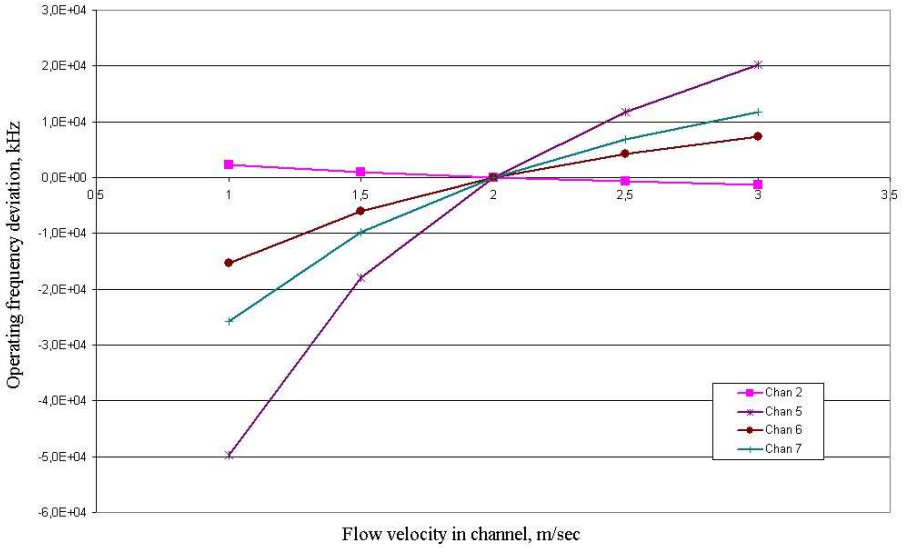


Figure 5.2: The Gun 4 cavity frequency shift sensitivity $\delta f_2 - \delta f_0, kHz$ to the flow velocity deviations in cooling channels. Reference flow velocity $V_0 = 2.0\frac{m}{sec}, P_a = 60kW$.

Fig. 5.3a where $E_1$ is the electric field strength at the cathode, $E_2$ is the maximal electric field value at the second cell axis. For a perfectly tuned RF Gun cavity the field values $E_1$ and $E_2$ should be equal.

In a coupled system the field balance at any cavity mode depends on the cells individual frequencies balance. The coupled circuit model parameters $\omega_1, \omega_2, \gamma_c$, see Fig. 5.3b, some equivalent definitions, introduced for a cavity model description and interpretation of results. In the experiments we measure field distributions and mode frequencies in the total cavity, which are the results of the cell modes interaction.

Suppose, we have equal fields in the Gun cavity cells, $|\frac{E_2}{E_1}| = 1.0$ and want to change them slightly by changing the cavity cooling condition. The Gun cavity has a **positive dispersion - increasing of the individual cell frequency leads to an increasing of the electric field in this cell** at the operating mode. Suppose, we have a reference operating cooling regime with the water flow velocity $V_0 = const$ in all channels. To increase the individual cell frequency, one has to decrease the cavity temperature at the chosen cell. For this purpose the water flow should be increased in the cooling channels, surrounding the cell. In Gun 4 cavity cooling channels $N1 \div N4$ surround the first cell and channels $N6 \div N11$ surround the second cell. Because the iris divides the cells, the cooling conditions in the iris channels should not be changed. Let us also suggest, we change the flow velocity in the corresponding channels simultaneously by the same amount. Such a change of the cooling for one cell leads to cell individual frequency change and operating mode frequency deviation with respect to reference frequency, $\delta f - \delta f_0$. The plots of the cavity operating frequency deviations for a cooling water flow velocity change in the range $(0.5V_0 \div 2.6V_0)$ are shown in Fig. 5.4a for a flow change in the channels $N1 \div N4$ and in Fig. 5.4b for channels $N6 \div N11$. The plots are shown for three cases of reference flow velocities $V_0 = 1.0\frac{m}{sec}; 1.5\frac{m}{sec}$, and $2.0\frac{m}{sec}$.

To couple an operating mode frequency shift and the field balance in the cells, we cannot use the ANSYS RF simulator, by directly considering the effect of a precise 3D cavity deformation onto the cavity frequency shift and field balance - this effect is far below the

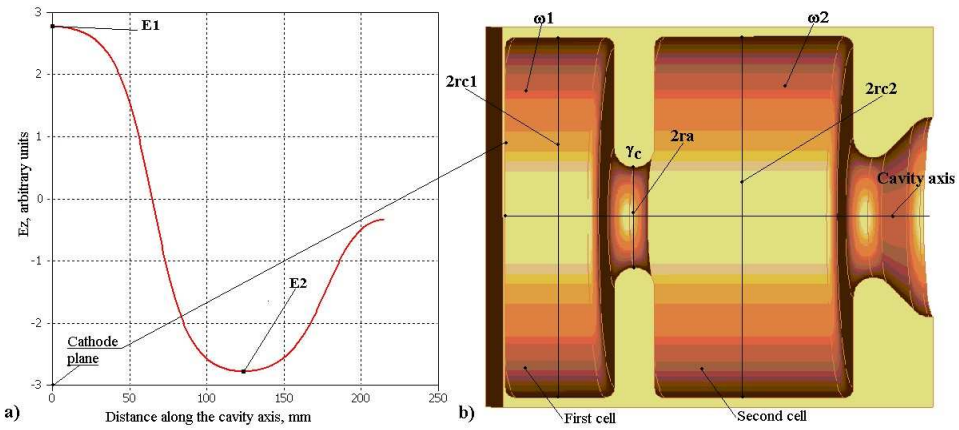


Figure 5.3: The typical electric field distribution along Gun cavity axis (a) and Gun cavity sketch with coupled model notations (b).

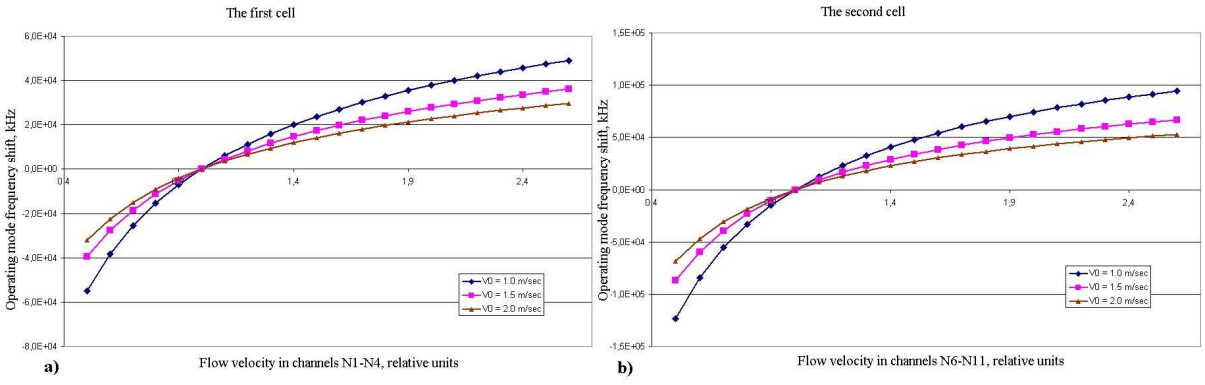


Figure 5.4: Operating mode frequency deviation for flow velocity change simultaneously in channels $N1 \div N4$ (a) and channels $N5 \div N11$ (b), $P_a = 60kW$.

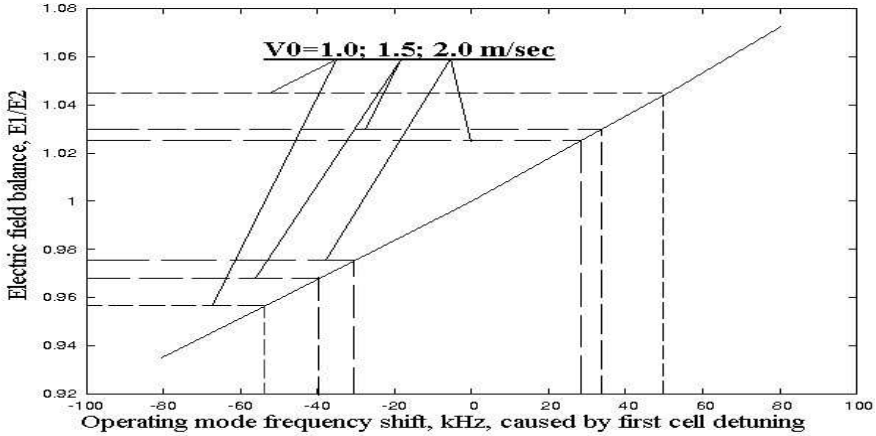


Figure 5.5: Field balance $\frac{E_1}{E_2}$ regulation range by changing the first cell own frequency.

precision of 3D FEM simulations. The cavity frequency shift, shown in Fig. 5.4, due to the change of the cells cooling conditions, is caused by the individual cell frequencies change. According to a coupled circuits model, the detailed reasons for a cell frequency change are not important for the determination of the field balance. We can choose a simplier way for the cell frequency detuning with the requirement to provide the same frequency shift and do not change the coupling coefficient $\gamma_c$. The operating frequency sensitivity to the cell radii $rc_1$ and $rc_2$ has been calculated by using Micro Wave Studio in the range $\pm 20\mu m$ with respect to the design values, showing a linear frequency dependence on $rc_1$ and $rc_2$. The sensitivity is different for the two cells - $\frac{\partial f_\pi}{\partial rc_1} = 5.35\frac{kHz}{\mu m}$ and $\frac{\partial f_\pi}{\partial rc_2} = 7.075\frac{kHz}{\mu m}$. It is a natural relation. The second cell has a bigger volume and more energy is stored in the operating mode. One can see the same effect comparing Fig. 5.3a and Fig. 5.3b.
During the RF Gun operation, the $\pi$-mode frequency should be constant. The operating frequency change, caused by the first cell detuning, should be compensated by an appropriate opposite detuning of the second cell. Due to a lower operating frequency sensitivity (and field balance as well) to the individual frequency of the first cell, **the range of a field balance control is defined by the first cell detuning.**

In Fig. 5.5 a plot of possible field balance control by a first cell detuning is shown. This plot needs more explanations. The $x$-axis shows an operating mode frequency shift, caused by the first cell detuning, under the assumption of a **constant frequency of the second cell.** This value is plotted because it can be measured and calculated easily. The $y$-axis shows the field balance (ratio $\frac{E_1}{E_2}$) **under the assumption of a constant operating frequency, i.e. the first cell detuning is compensated, with an appropriate** $rc_2$ **choice, by the required second cell detuning.**From Fig. 5.4 and Fig. 5.5 one can estimate the range of possible field balance change. As one can see from Fig. 5.4a, a change of the flow velocity in channels $N1 \div N4$ from $0.5V_0$ to $2.6V_0$ results in a shift of the operating mode frequency from $-55.1kHz$ to $49.06kHz$ for a reference velocity of $V_0 = 1.0\frac{m}{sec}$, from $-39.61kHz$ to $36.05kHz$ for $V_0 = 1.5\frac{m}{sec}$ and from $-32.07kHz$ to $29.6kHz$ for $V_0 = 2.0\frac{m}{sec}$. From the plots in Fig. 5.4b one can find the required change of the flow velocity in channels $N6 \div N11$ to compensate the operating mode frequency shift. And from the plot in Fig. 5.5 one can find that the described flow velocity changes result in a possible field balance change from $\frac{E_1}{E_2} = 0.956$ to 1.042 for the reference velocity $V_0 = 1.0\frac{m}{sec}$, from 0.97 to 1.03 for $V_0 = 1.5\frac{m}{sec}$

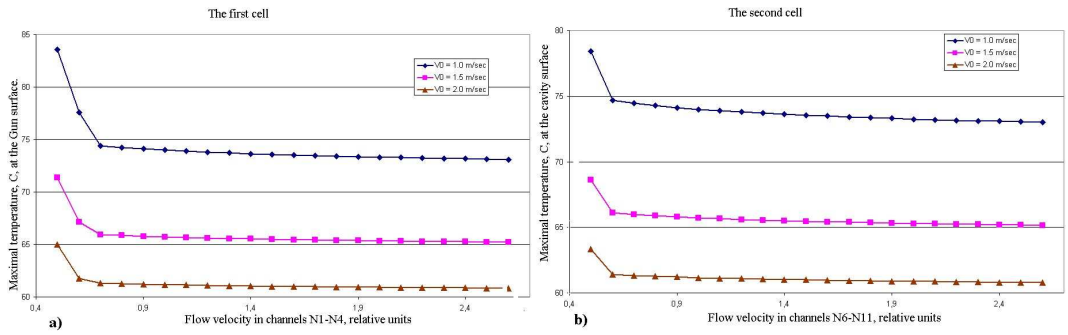


Figure 5.6: The maximal temperature, $C^o$, at the cavity surface for flow velocity change simultaneously in channels $N1 \div N4$ (a) and channels $N5 \div N11$ (b), $P_a = 60kW$.

and from 0.976 to 1.024 for $V_0 = 2.0\frac{m}{sec}$.
A wider range of field balance control is realized for a lower reference flow velocity. But a lower reference flow velocity leads to a larger cavity frequency shift for the given dissipated RF power. The possibility of a wide range of the field balance control is in contradiction to the requirement of the maximal possible dissipated RF power.
The presented data for a field balance control are for the existing Gun 4 cavity geometry. If this option - field balance control - is one of the goals for future Gun cavities, the cavity geometry must be changed. To increase the field balance sensitivity to the deviations of the individual cell frequencies, we have to decrease the coupling coefficient. From the theory of coupling through a round hole [4] it is known that $\gamma_c \sim r_a^3$, where $r_a$ is the inner iris radius, see Fig. 5.3b. But, with a decreased coupling coefficient, and hence improved field balance control range, we decrease the mode separation $\omega_\pi - \omega_0$ and increase the field balance sensitivity to the cavity manufacturing and tuning errors. Such an RF Gun cavity will be more difficult in the preliminary RF tuning.

Another important point for the change of field balance by a control of the cooling regime is the maximal temperature at the cavity surface. For reference we note, that the cooling with the same flow velocity in all the channels leads to a point with the maximal surface temperature at the iris. A simultaneous reduction of the flow velocity in channels $N1 \div N4$ or $N6 \div N11$ in order to detune cell frequencies, leads to an increase of the surface temperature in the first or second cell, respectively. The plots of maximal surface temperature for a simultaneous flow velocity change in the corresponding channels is shown in Fig. 5.6. As one can see, for a large flow velocity reduction to $0.5V_0$ the point of maximal surface temperature moves from the iris to the back part, for a flow reduction in channels $N1 \div N4$, Fig. 5.6a, and to the front part, for a flow reduction in channels $N6 \div N11$, Fig. 5.6b. For a lower reference flow velocity the surface temperature increase is stronger. For the reference flow velocity $V_0 = 2.0\frac{m}{sec}$ this increase of the maximal surface temperature is not essential.

# 6 Summary

Possibilities of optimization and particularities for the cooling regimes in the existing DESY Gun cavities N2, N3 and N4 have been studied in wide range of flow rates by means of numerical cavity parameters simulations. The investigation of a flow rate redistribution

between the two sub circuits in Gun 3 and Gun 2 shows no local extremum - an increase of the flow rates in each sub circuit leads to a decrease of the cavity frequency shift. A flow velocity range of $\approx (2.0 \div 3.0) \frac{m}{sec}$ is most reasonable. For lower velocities the cavity frequency shift rises fast with decreased velocity and with a high sensitivity to velocity deviations. A flow velocity increase to $\approx (4.0 \div 5.0) \frac{m}{sec}$ does not lead to proportional decrease of the cavity frequency shift.
From the point of view of the cavity frequency control, the maximal dissipated average RF power is $\approx 100kW$ for all Gun cavities even for moderate flow velocities $\approx (2.0 \div 3.0) \frac{m}{sec}$ and is limited by the tolerable cavity surface temperature.
The cooling circuit design for Gun 3 cavity with two turn channels in the cylindrical sub circuit is more effective with respect to the total water consumption, as compared to the Gun 2 cylindrical sub circuit design with one turn channels.
A rigid stainless steel jacket is a useful part the of DESY Gun cavity design. The restriction of the cavity expansion in radial direction leads to a decreased cavity frequency and, finally, results in a larger value of dissipated RF power for the same cavity frequency shift.
The Gun 4 cooling circuit design with independent cooling channels allows a fine field balance control (in the range of several percent) by a change of the cell cooling. The range of possible field balance control decreases with increased dissipated RF power and related increased total flow rate.

# 7 Acknowledgements

The authors thank the PITZ group, especially M. Krasilnikov, S. Korepanov, B. Petrosyan, T. Scholz, for fruitful discussions and help in providing measurement data.

# References

[1] S.C. Joshi et al., The complete 3D coupled RF-thermal-structural-RF analysis ... LINAC02, p. 216, 2002.

[2] F. Marhauser. Finite Element Analyses for RF Photoinjector Gun Cavities.TESLA FEL, Report 2006-02, DESY, 2006.

[3] L.D. Landau, E.M. Lifshiz. Theoretical physics. Theory of Elasticity.Moscow, Nauka, 1988.

[4] R. M. Bevensee. Electromagnetic slow wave systems. John Wiley Inc., New York, 1964.